Available online at www.sciencedirect.com
SCIENCE DIRECT®
Cement & Concrete Composites 26 (2004) 967–976
Cement & Concrete Composites
www.elsevier.com/locate/cemconcomp

# The chemical composition and microstructure of hydration products in blended cements

J.-I. Escalante-Garcia [1], J.H. Sharp *

*Department of Engineering Materials, Sir Robert Hadfield Building, University of Sheffield, Mappin Street, Sheffield S1 3JD, United Kingdom*

**Abstract**

Pastes of neat and blended Portland cement (incorporating either 60% ground granulated blast furnace slag, or 30% pulverised fuel ash, or 22% volcanic ash) were cured for one year at temperatures ranging from 10 to 60 °C. The hydration products were characterised by X-ray diffraction, scanning electron microscopy and energy dispersive spectroscopy. The apparent porosity of the pastes increased with increasing curing temperature. Chemical analysis data for the hydration products are presented in ternary composition diagrams, where it is noted that in the presence of the replacement materials the composition of the C–S–H shifted towards higher Si and Al contents, whereas that of Ca was lower.


*Keywords:* Chemical composition; Microstructure; Temperature dependence; Backscattered electron imaging; Blastfurnace slag; Pulverised fuel ash; Volcanic ash

## 1. Introduction

Portland cement is the essential binding agent in concrete, which in turn is the most widely used construction material worldwide due to its many advantages, including lower cost (relative to steel, aluminium or polymers), durability and other properties. Materials of natural origin such as volcanic ash (VA), or industrial by-products, like ground granulated blast furnace slag (GGBS) and pulverised fuel ash (PFA), have been widely used as partial replacement of Portland cement in concrete constructions. The advantages include improved technological properties, low cost and a reduction in the environmental impact through reduction of waste accumulation. Furthermore, the simple replacement of 5% of cement by one of the aforementioned materials can provide a reduction of about $75\times10^6$ tons of $CO_2$ (considering a world production of about $1500\times10^6$ tons/year with emission of an average 1 kg $CO_2$/kg cement).

The understanding of the chemistry of the hydration of Portland cement is still an area of opportunity for many researchers. The addition of replacement materials to Portland cement brings additional complexity to the chemical reactions developed during the hydration of the composite cements. In recent years it has become apparent that both latently hydraulic and pozzolanic materials participate in the overall hydration process and development of microstructure. The dominant product of these reactions is C–S–H gel, which is principally responsible for the mechanical properties of the hydrated cement. C–S–H gel is generated by the interaction of the replacement materials with portlandite, CH, liberated during the hydration of the alite and belite present in the cement [1].

There are few previous studies of the effect of curing temperature on the rate and degree of hydration and the development of microstructure in neat and blended cement, with the notable exception of those by Kjellsen, Detwiler and colleagues [2–5], who reported the effects of curing temperature on reactivity in terms of non evaporable water, porosity and microstructural development. The principal observations and conclusions from our previous papers [6–10] are summarised below, and it can be seen that the results agree well with theirs where comparable, but also extend their study through the use of quantitative X-ray diffraction, isothermal conduction calorimetry, and in other respects.

* Corresponding author. Tel.: +44-114-222-5504; fax: +44-114-222-5943.
*E-mail address:* j.h.sharp@sheffield.ac.uk (J.H. Sharp).
[1] Current address: Center for Research and Advanced Studies (Cinvestav) IPN, Saltillo Unit, Carretera Saltillo-Monterrey Km 13 Saltillo, Coahuila CP 25900, Mexico.

0958-9465/$ - see front matter © 2004 Elsevier Ltd. All rights reserved.
doi:10.1016/j.cemconcomp.2004.02.036

### 1.1. Neat cements

An increase in the curing temperature brought about acceleration of the early hydration of the anhydrous phases present in the cement, but to differing extents [6]. A temperature inversion was established for the hydration of the alite and ferrite phases, with the lowest ultimate degree of hydration (DoH), amount of CH formed, and compressive strength being observed at the highest curing temperature [6].

After curing for 1 year at 60 °C, there was greater apparent porosity, as observed in backscattered electron images (BEI), than at 10 °C [6,7]. The partially hydrated grains were lighter grey in colour at 60 °C and there were some rims of discontinuity around some of these grains. The microstructure after curing at 10 °C for 1 year was more homogenous and notably lower in porosity, leading to the higher compressive strength already noted [6,7]. As the curing temperature increased, the S/Ca ratio increased significantly, whereas the Al/Ca and (Al + Fe)/Ca ratios of the inner products decreased [8]. It was suggested that S, probably in the form of sulfate ions, can be sorbed by the C–S–H gel at elevated curing temperatures [8]. AFm clusters formed from the hydration of $C_3A$ were observed in the microstructure of pastes cured for one year at 10 °C, but not in those cured at 60 °C [6].

Isothermal conduction calorimetry studies have been fully reported [9], but an illustrative set of curves for OPCN hydrated at 10, 30 and 60 °C are shown in Fig. 1. An increase in curing temperature caused peak II, which is associated with the hydration of the alite phase, to be of greater intensity and shifted to earlier times, while peaks II and III tended to merge, so that peak III was more evident on curing at 30 °C than at 60 °C [9]. Beyond 30 h, the cements cured at the lower temperatures continued to evolve heat to a greater extent than those cured at higher temperatures, leading eventually to the temperature inversion effect noted above [9].

### 1.2. Blended cements

There was an increase in the DoH of the cement fraction in the blended cement pastes compared with that in the neat cements [7]. In particular, the DoH of alite greatly increased from very early stages of the reaction in the presence of GGBS and VA, but to a much lesser extent when PFA was present [10]. The temperature inversion effect noted for the neat cements was also evident in the blended cements [10].

The presence of 60%GGBS in the blended cement made a clear contribution to the heat evolution detected by ICC as shown in Fig. 1. An additional peak (referred to as peak S) was observed after peak II at all the curing temperatures investigated, and was more completely separated from peak II at lower temperatures. Peak S is attributed to the hydration of the slag component, resulting from the liberation of CH from the hydration of alite [9]. The hydration of the ferrite phase was also dramatically accelerated by the presence of GGBS, whereas the acceleration was apparent to a lesser extent in the presence of VA and PFA [10]. The temperature inversion in the rate of hydration of the ferrite phase was observed for all three blended cements [10].

Higher curing temperatures favoured the pozzolanic reaction, resulting in the maximum amounts of CH formation being shifted to lower values and shorter times as the curing temperature increased [10]. In the

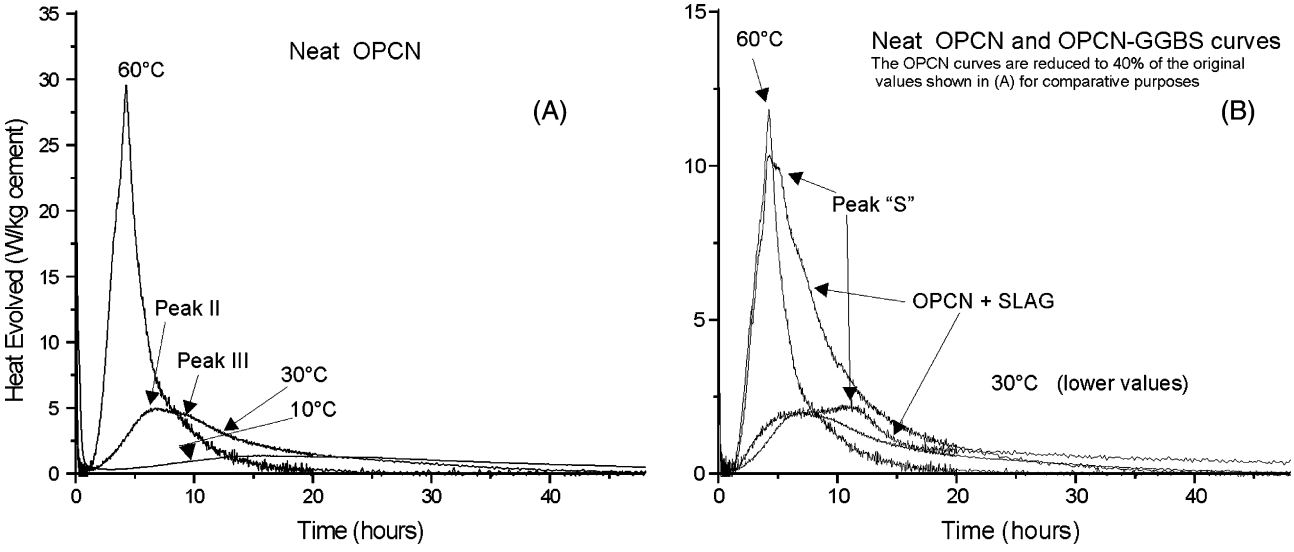


Fig. 1. Isothermal conduction calorimetry curves for (A) OPCN hydrated at 10, 30, 60 °C and (B) 40%OPCN–60%GGBS and neat OPCN cements cured at 30 and 60 °C.

microstructure of the pozzolanic cement pastes cured at 60 °C, CH was almost absent, whereas after curing at 10 °C, some CH clusters were visible [7]. The ICC study [9] suggested that incorporation of low-lime PFA caused retardation of the initial hydration of the cement fraction, although it subsequently brought about enhanced reactivity of the anhydrous alite. The presence of a peak S similar to that observed in the GGBS system, confirmed that the VA was involved in the overall hydration process [9]. Alkali released from the hydration of alite activated the reaction of the VA, resulting in greater heat evolution from the cement fraction [9].

### 1.3. Aims of the present study

Energy dispersive spectroscopy (EDS) has been used to analyse the reaction products that formed during the hydration of both the neat and blended cements. Data for the neat cements have been plotted previously [7] in the manner developed by Taylor and his co-workers [11]. This approach depends upon the use of atomic ratios, usually involving the amount of calcium present, to overcome the problem that the sum of the elemental contents is frequently much less than 100% because of the water content that cannot be analysed by EDS. An alternative approach has been developed by Bonen and Diamond [12]. In this method, the analyses were converted to atomic proportions and then normalised to 100%. Open-sided ternary composition diagrams were used to present the data, enabling conclusions to be drawn about actual compositional data and their variations among the phases present in intimate mixtures within the cement matrix. In this paper, some of the data already published on the neat cements is re-examined using an approach similar to that of Bonen and Diamond, along with much new data obtained from BEI-EDS examination of the microstructure developed in the blended cement systems after curing for one year at 10 °C, 30 °C and 60 °C. Emphasis is given to analysing the changes in the chemical composition of the C–S–H formed in the presence of the three replacement materials.

Another difference in nomenclature has arisen in recent years in that some authors (e.g. Taylor [1]) refer to inner products (IP) and outer products (OP), whereas others (e.g. Diamond and Bonen [13]) refer to phenograins (pheno from the Greek for distinct) and groundmass. Taylor [1] defines inner products as the gel formed in situ from the large anhydrous grains, as opposed to the outer products found in the space that was originally water-filled. Diamond and Bonen use the term phenograin to describe any individual grains of 10 μm or larger embedded in the groundmass, which includes smaller particles and pore space. The IP/OP nomenclature is used in this paper, but all the material described here as IP, and also the AFt and CH crystals observed, would meet Diamond and Bonen's definition of phenograins.

## 2. Experimental

### 2.1. Materials

Two Portland cements were kindly supplied by the Mexican company Cementos Apasco and designated OPCN and OPCS to indicate the different (North and South) plants from which they originate. They differ significantly in chemical and mineralogical composition, so that OPCS is a typical normal or ordinary Portland cement, whereas OPCN tends in composition towards a sulfate-resisting Portland cement. Mexican volcanic ash (VA) and pulverised fuel ash (PFA), and U.K. ground, granulated blastfurnace slag (GGBS), supplied by Frodingham Cement Company, were used in this investigation to make three blended cements: 70%OPCN–30%PFA, 40%OPCN–60%GGBS, 78%OPCS–22%VA. The chemical analyses of all these materials are presented in Table 1, and additional information about them has been published previously [6,10].

### 2.2. Experimental procedure

Pastes with a water/solids ratio of 0.5 were prepared for all cements and cast into bars ($10\times10\times100$ mm). After 24 h at 20 °C under high humidity conditions the bars were transferred to water baths at 10, 30 and 60 °C for curing. X-ray diffraction patterns were obtained using a Siemens D500 diffractometer over the range from 5 to 60 °C with a step of 0.05° $2\theta$ and with a measuring time of 20 s, as described previously [6]; the samples were ground in a ball mill for 20 min and back-loaded in the sample holder to minimize preferential orientation of CH. After curing for one year, fragments of the bars were dried under vacuum for 24 h, further mounted in resin, polished down to 0.25 μm and carbon coated for analysis under scanning electron microscopy (Cambridge CamScan, Cambridge UK) operated at 20 kV and equipped with microanalysis capabilities. ZAF corrections were performed by the equipment software. The EDS analyses were performed on the hydration products and grouped as those formed inside the partially or fully hydrated cement grains (inner products, IP) and those deposited in the spaces initially occupied by water (outer products, OP). The results are presented as ternary diagrams Ca–Si–Al, Ca–S–(Al + Fe) and Ca–Al–Mg in which the totals of the three or four elements considered were plotted as normalised to 100%. It should be noted that this procedure differs from that used by Bonen and Diamond [12], who normalised the analysis of all the elements determined to 100%, but in practice the differences are not great.

Table 1
Oxide and potential phase composition (from QXDA) of the starting materials (glass fraction calculated by difference)

| | OPCN | OPCS | OPCVA | GGBFS | PFA | Volcanic ash |
|---|---|---|---|---|---|---|
| CaO | 63.6 | 64.4 | 49.4 | 41.1 | 1.9 | 1.0 |
| $SiO_2$ | 20.6 | 20.9 | 31.9 | 32.9 | 64.2 | 68.2 |
| $Al_2O_3$ | 4.6 | 5.7 | 6.9 | 12.6 | 26.5 | 11.2 |
| $Fe_2O_3$ | 3.1 | 2.9 | 2.7 | 0.5 | 4.4 | 1.8 |
| $Na_2O$ | 0.5 | 0.6 | 0.9 | 0.3 | 0.1 | 0.2 |
| $K_2O$ | 0.9 | 0.6 | 1.5 | 0.7 | 1.1 | 3.4 |
| MgO | 1.6 | 1.9 | 1.4 | 8.4 | 0.7 | 0.2 |
| $SO_3$ | 3.5 | 2.4 | 3.2 | 2.2 | 0.3 | 0 |
| C | 0.16 | 0.18 | 0.26 | 0.23 | 1.34 | 0.04 |
| Ins. res. | 0.35 | 0.6 | 20.3 | | | |
| LOI | 0.9 | 0.6 | 2.2 | | 1.6 | |
| Total | **99.5** | **100.4** | **100.4** | **98.9** | **100.6** | **86.1** |
| Free lime | 1.1 | 1.0 | 1.0 | | | |
| $C_3S$ | 71.6 | 65.6 | 48.6 | | | |
| $C_2S$ | 10.9 | 16.4 | 10.5 | | | |
| $C_3A$ | 3.7 | 8.0 | 6.0 | | | |
| $C_4AF$ | 10.7 | 7.4 | 6.0 | | | |
| Other | 2.7 | 1.9 | 6.0 | | | |
| Quartz | | | | 1 | 11.0 | |
| Mullite | | | | | 18.0 | |
| Magnetite | | | | | 1.5 | |
| Melilites | | | | 1 | | |
| Glass | | | | ≈98 | ≈69.5 | |

## 3. Results and discussion

### 3.1. Microstructure of neat Portland cement cured at various temperatures for 1 year

The microstructure of OPCS cured at 30 °C for 360 days is shown in Fig. 1 at relatively low magnification. Because elements with higher atomic number appear brighter in BEI, variations in the grey level of the phases present can be observed. In descending order of brightness, the anhydrous phases, calcium hydroxide, C–S–H gel and porosity (which appears black) can be distinguished [14,15], as indicated in Fig. 2. Further BEI micrographs contrasting the microstructure that developed after curing for 1 year at 10 and 60 °C have been published elsewhere [6]. Although the rate of hydration was initially faster at 60 °C than at 10 °C, the degree of hydration after 1 year was greater at 10 °C than at 60 °C and some fully hydrated grains could be identified. At 30 °C, as clearly visible in Fig. 2, some partially hydrated cement grains could be identified as a grey rim of inner hydration products (labelled IP in Fig. 2) formed around a white core of anhydrous cement.

EDS analyses for a total of 225 compositions within the inner hydration products and 204 compositions from the outer products of OPCN and OPCS pastes are plotted as atomic percentages, normalised to 100%, in a Ca–Si–Al ternary diagram in Fig. 3. The other elements present, primarily Fe and S, but also including K, Na and Mg, are ignored. The data relate to both of the neat

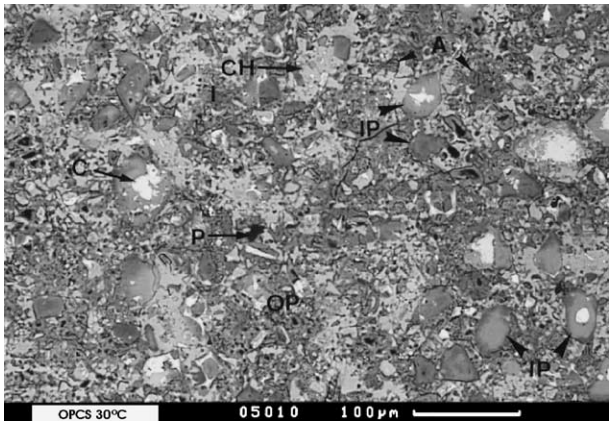


Fig. 2. BEI of OPCS cured at 30 °C for 1 year. C = anhydrous cement grain, CH = $Ca(OH)_2$, IP = inner product, OP = outer product, P = porosity.

cements hydrated for 1 year at 10, 30 and 60 °C. Although we have previously reported the effect of temperature [8] on the composition of the inner products of both cements, they all seem to fall within a compact range of composition. Standard deviations relative to the average values were 3.4%, 5.8% and 34% for Ca, Si and Al respectively, in inverse relationship to the amount of the element present in C–S–H. The average normalised analysis was Ca, 0.66; Si, 0.31; Al, 0.03; leading to a high Ca/Si ratio of 2.13.

The analyses of the outer products plotted differently. While some were located close to the cluster of analyses

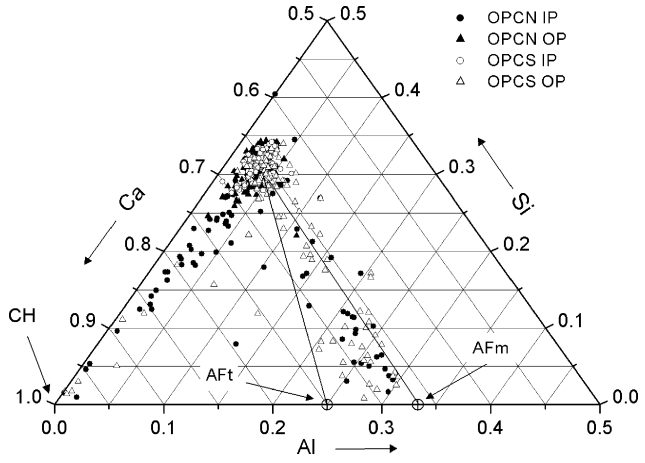


Fig. 3. Ca–Si–Al ternary diagram for OPCs cured for 1 year at 10, 30 and 60 °C.

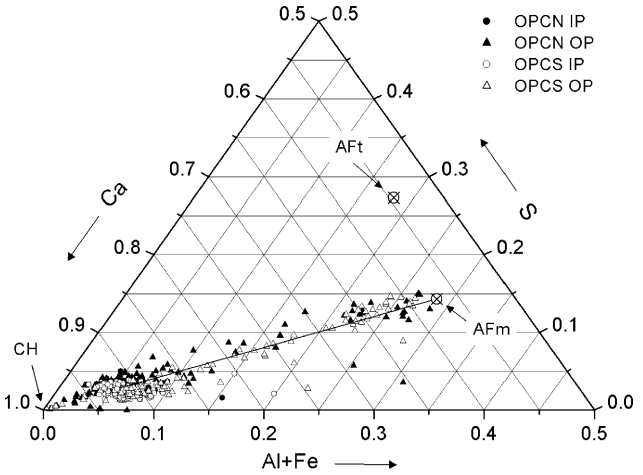


Fig. 4. Ca–S–(Al + Fe) ternary diagram for OPCs cured for 1 year at 10, 30 and 60 °C.

from the inner products, others were scattered in two general directions. The first connected the composition of C–S–H to that of portlandite, marked CH in Fig. 3 and corresponding to the Ca vertex of the ternary diagram. The analyses extended almost parallel to the axis, all the way between the two extremes of composition. These analyses are believed to correspond to a fine intimate mixture of C–S–H and CH formed in space originally occupied by water. The second general direction was towards the composition of the two sulfate-containing phases, ettringite or AFt, $Ca_3Al_2O_6 \cdot 3CaSO_4 \cdot 32H_2O$, and monosulfate or AFm, $Ca_3Al_2O_6 \cdot CaSO_4 \cdot 12H_2O$, with some substitution of Al by Fe possible in both phases. Many points plotted on or close to the line connecting the composition of C–S–H to that of AFm, but a substantial number of other points plotted between the two lines. X-ray diffraction indicated the presence of both phases and since no AFt crystals were noted in the microstructures it is concluded that it must be finely intermixed with the C–S–H.

The same experimental data for the two neat Portland cements are plotted in the Ca–S–(Al + Fe) ternary diagram shown in Fig. 4. Note that this plot does not include the Si data, but instead includes S and Fe, the latter grouped with Al. The ideal compositions for AFt and AFm are indicated. The data from the analyses of the inner products gathered into a cluster close to the 100% Ca vertex of the diagram and with a low content of S (normalised average value of 0.027% atomic with standard deviation 26% of the average). All the data from the analyses of the outer products lay along the line joining the inner product cluster with the AFm composition. These data are much less scattered than those shown in a similar plot by Bonen and Diamond [12], but their data relate to a cement cured for only 3 days, whereas the present results are after curing for 1 year. A few points were positioned at or near 100% Ca, which represents the composition of CH. From Figs. 3 and 4, it seems clear that the hydration products are similar for the two cements (from different manufacturing plants and in spite of their somewhat different mineralogical analyses) and for different curing temperatures (10, 30 and 60 °C). An alternative way of plotting these data has been shown elsewhere (Fig. 3 of [8]).

### 3.2. Microstructure of an OPC–GGBS blended cement cured at various temperatures

When a fraction of the Portland cement is replaced by a pozzolanic or a latently hydraulic material, a notable change in the rate of hydration of the anhydrous cement phases and in the consumption of the portlandite generated by the hydration of the alite is observed [1,10]. BEI micrographs of the microstructure developed by 40%OPCN–60%GGBS blended cement cured at 10 and 60 °C for 1 year are shown in Fig. 5(A) and (B), respectively. Similar micrographs have been published previously [7]. The blastfurnace slag grains can be distinguished from the cement grains by their more angular morphology and because they are slower to react. Some reacted slag grains exhibited rims of hydration products formed within the boundaries of the original slag grains at 60 °C (and also at 30 °C), although some dissolution could have taken place in the alkaline environment. The rate of consumption of the GGBS is strongly dependent on the curing temperature; at 10 °C most of the slag grains had only reacted slightly, whereas at 60 °C, some slag grains were fully hydrated (Fig. 5). These differences are partly due to kinetics, because the rate of reaction is greater at the higher temperature, but there may also be a change in reaction mechanism. At 60 °C the GGBS grains shown in Fig. 5B seem to be consumed from

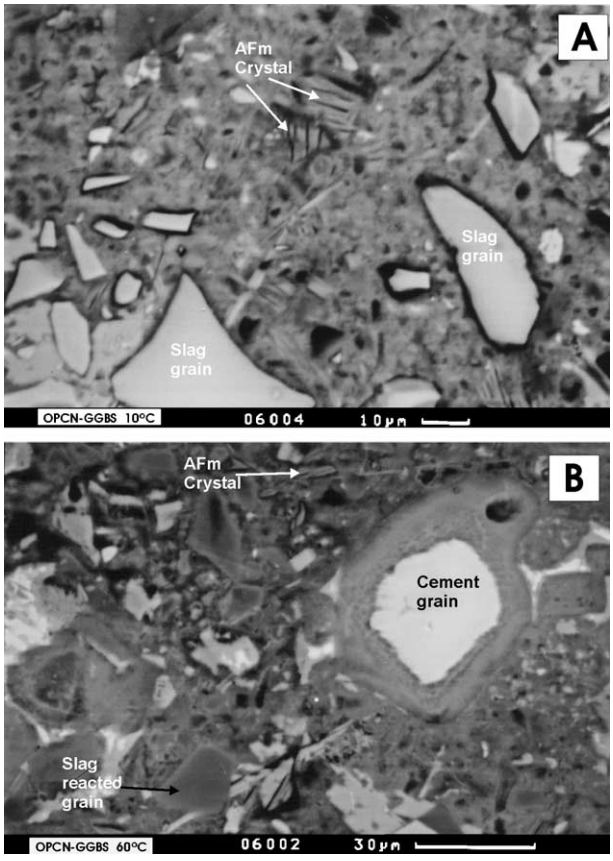


Fig. 5. BEI of OPCN–GGBS cured for 1 year at (A) 10 °C, (B) 60 °C.

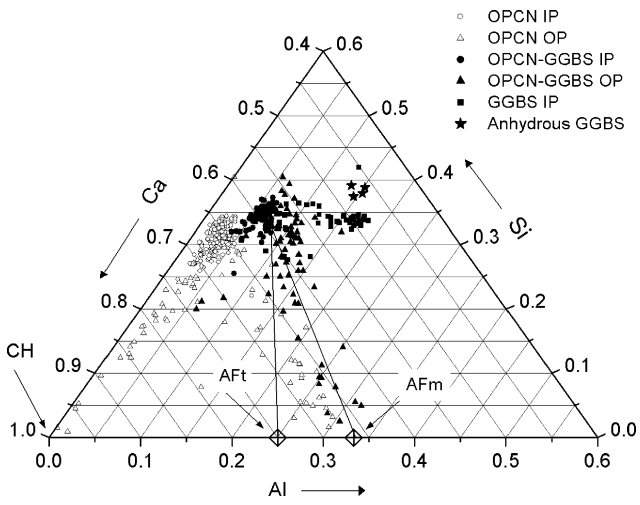


Fig. 6. Ca–Si–Al ternary diagram for OPC and OPC–GGBS cured for 1 year at 10 and 60 °C.

the surface of the grains inwards, whereas at 10 °C a dissolution–precipitation mechanism seems to predominate. Further related observations have been made recently in alkali activated slag systems over a similar range of temperatures [16].

X-ray diffraction and thermogravimetric analysis [7] of the OPCN–GGBS pastes indicated the presence of portlandite, monosulfate and a hydrotalcite-like phase at both curing temperatures, but more monosulfate and less portlandite were evident at 60 °C. Ettringite was observed at 10 °C, but in only very small amounts at 60 °C; it was not apparent in the SEM investigation, but AFm crystals were identified by EDS and were relatively abundant at both curing temperatures (see Fig. 5). Calcium hydroxide was rarely observed by SEM and indeed little was present, confirming the observations made by Escalante et al. [17] and Hill and Sharp [18] that at various moderate to high levels of replacement (30% and 50% in [17]; 75% and 90% in [18]; 60% in the present study) GGBS acts as a pozzolanic material, reacting with the CH grains to form more C–S–H gel.

In Fig. 6, the EDS analyses are plotted for both the Portland cement OPCN and for the OPCN–GGBS blended cement in a Ca–Si–Al ternary composition diagram. The analyses of the inner products from the hydration of the blended cement gathered in a cluster, but this was displaced from the comparable cluster formed by the analyses of the neat cements. The IP of the slag cement had higher contents of Al and Si, but a lower content of Ca than that of the neat cement, with an average composition, Ca, 0.60; Si, 0.34; Al, 0.06. The Ca/Si ratio had decreased from 2.13 to 1.76 in the presence of the GGBS. This deficiency in calcium is associated with its consumption by reaction with GGBS to form additional C–S–H gel, in view of its lower calcium content compared with that of Portland cement.

The analyses of the outer products from the GGBS blended cement were grouped in two regions; the first in a cluster close to the OPCN–GGBS inner products and the second close to the line connecting this cluster with the composition of AFm on the Al-axis. This observation is in accordance with the greater amount of AFm relative to AFt indicated by X-ray diffraction, as noted from the intensity of the peaks. The data points relating to the hydration products formed within the slag grains on curing at 60 °C (labelled GGBS IP in Fig. 6) formed another cluster with a different composition from both of the Portland cement inner products clusters. They had variable Al contents, but the Si and Ca contents were relatively constant, with a lower Ca/Si ratio than that in the cement IP. These points are not, in fact, too far away from the composition of the anhydrous GGBS, which is also shown in Fig. 6.

Ternary composition diagrams can also be used to understand the nature of the other hydration products of OPC–GGBS as shown by XRD. A plot of the OPC–GGBS compositions on the Ca–S–(Al + Fe) axes as used in Fig. 4 is shown in Fig. 7. In this figure, three regions in the microstructure of OPCN–GGBS are distinguished, namely the inner products of the cement grains, the inner products of the slag grains, and the outer products. The inner products of the OPC grains in the

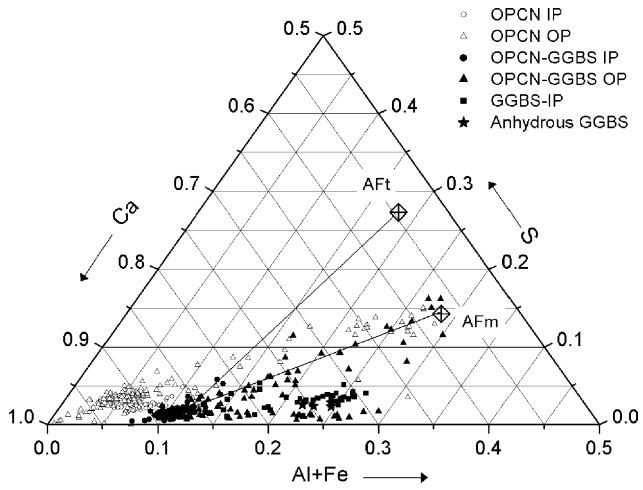


Fig. 7. Ca–S–(Al + Fe) ternary diagram for OPC and OPC–GGBS cured for 1 year at 10 and 60 °C.

blended cement tended to have a lower Ca content but higher (Al + Fe) content than those in the neat cement, while the (Al + Fe) content of the inner products in the slag grains was higher again. All such inner products showed similarly low S contents. Many of the analyses of the outer products again lay close to a line connecting the composition of the C–S–H to that of AFm, whereas there were no points extending towards AFt.

A ternary plot of a kind not previously shown is provided in Fig. 8 for OPC and OPC–GGBS pastes. In this figure the analytical results for the Ca–Al–Mg compositional field are plotted, which are of interest because Mg is a major component of GGBS. The analyses of the blended cement outer products and especially the inner products within the original slag grains show appreciably higher magnesium contents than found in the OPC. In fact, there is a clear linear progression from the composition of C–S–H (shown in Fig. 8), but this does not correspond to the theoretical line, also shown, connecting the composition of C–S–H to that of hydrotalcite, $Mg_6Al_2(CO_3)(OH)_{16}\cdot 4H_2O$, which was observed by XRD. Hydrotalcite like phases are commonly reported in alkali activated GGBS [19]. The composition of hydrotalcite is, however, quite variable and allows extensive solid solution [1,20]. The composition of the hydrotalcite-like phase formed in this composite cement seems to have a Mg:Al ratio lower than that in the ideal formula. The composition of the anhydrous slag actually lies quite close to the line drawn through the experimental data. It is clear from Fig. 8 that formation of a hydration product containing both Mg and Al probably takes place within the confines of the original slag grains. The outer products are comprised of very finely intermixed C–S–H gel, AFm and a hydrotalcite-like phase.

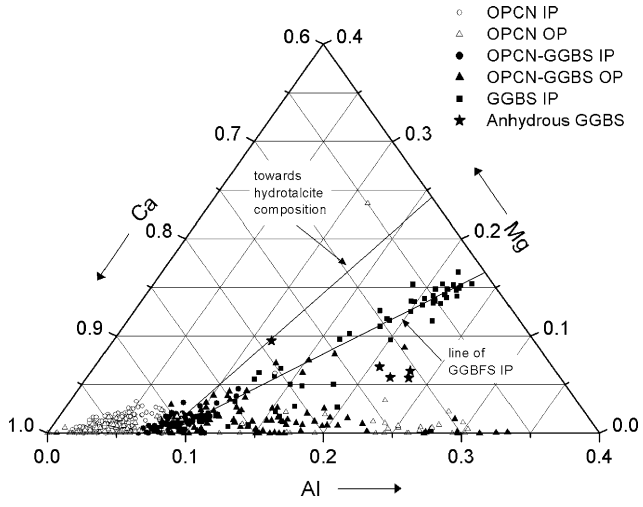


Fig. 8. Ca–Al–Mg ternary diagram for OPC and OPC–GGBS cured for 1 year at 10 and 60 °C.

### 3.3. Microstructure of an OPC–VA blended cement cured at various temperatures

BEI of the OPCS–VA blended cement after curing for 1 year at 10 and 60 °C are shown in Fig. 9A and B, respectively, confirming the general pattern of behaviour reported previously [7] where several scanning electron micrographs were shown after hydration at 10, 30 and 60 °C. The microstructure observed after curing at 10 °C indicates a high degree of hydration of the anhydrous phases in the cement and low porosity [7,10], whereas the porosity after curing at 60 °C is appreciably greater.

The Ca–Si–Al ternary diagram, shown in Fig. 10, once again indicates that many of the outer product analyses lie close to a line connecting the composition of the C–S–H to that of AFm. The presence of AFm was indicated by XRD and observed by SEM in the hydration products at 10 and 30 °C. There are only a few points connecting C–S–H to CH (the vertex at which Ca = 1) because the portlandite formed is known to be consumed by the pozzolanic reaction that is taking place [10]. The Ca–S–(Al + Fe) ternary diagram, shown in Fig. 11, also indicates that the outer products are an intimate mixture of C–S–H and AFm.

### 3.4. Microstructure of an OPC–PFA blended cement cured at various temperatures

BEI of PFA blended cement have been shown elsewhere [7] and were similar to those published by many other authors and summarised by Taylor [1].

The presentation of EDS analyses in ternary composition diagrams is, however, still novel, and such plots for the OPC–PFA blended cement are presented in Figs. 12 and 13. In the Ca–Si–Al diagram (Fig 12), the chemical composition of the cement fraction inner products is quite different from that of the neat cement, having lower Ca and higher Si and Al contents. The

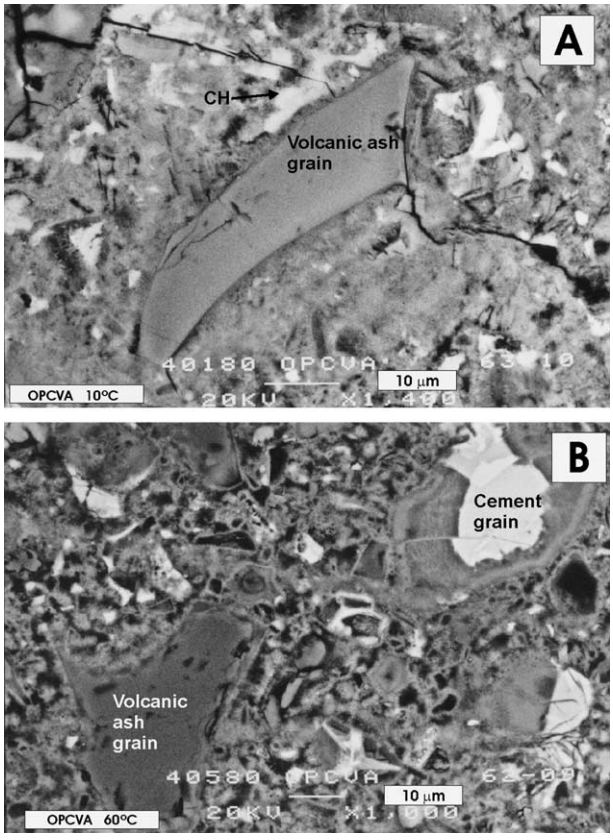


Fig. 9. BEI of OPCS–VA cured for 1 year at (A) 10 °C and (B) 60 °C.

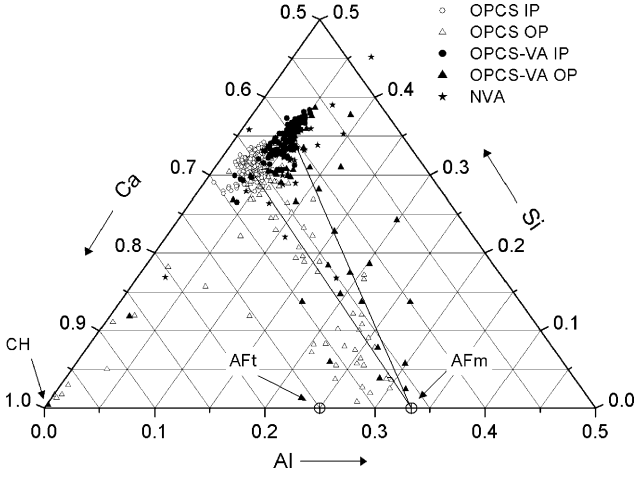


Fig. 10. Ca–Si–Al ternary diagram for OPCS and OPCS–VA cured for 1 year at 10, 30 and 60 °C.

outer products lay in a region bounded by the compositions of C–S–H, AFm and AFt. The analyses taken in the vicinity of the PFA grains (labelled NPFA in Figs. 12 and 13), along with some analyses of the outer products, plotted in a quite different direction. The trend displayed here was between the compositions of the anhydrous PFA and that of stratlingite, $C_2ASH_8$, a

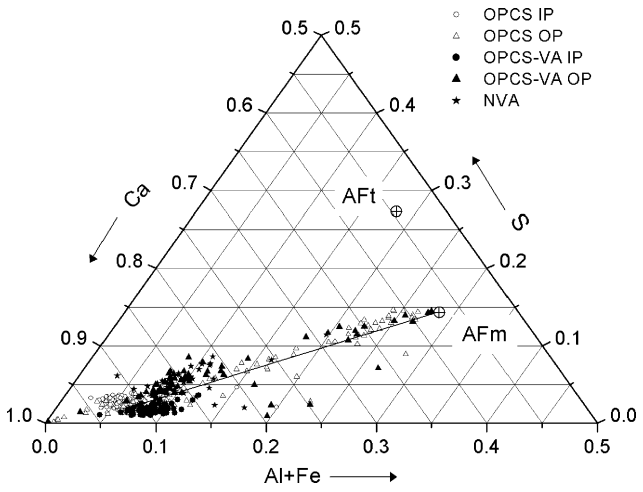


Fig. 11. Ca–S–(Al + Fe) ternary diagram for OPCS and OPCS–VA cured for one year at 10, 30 and 60 °C.

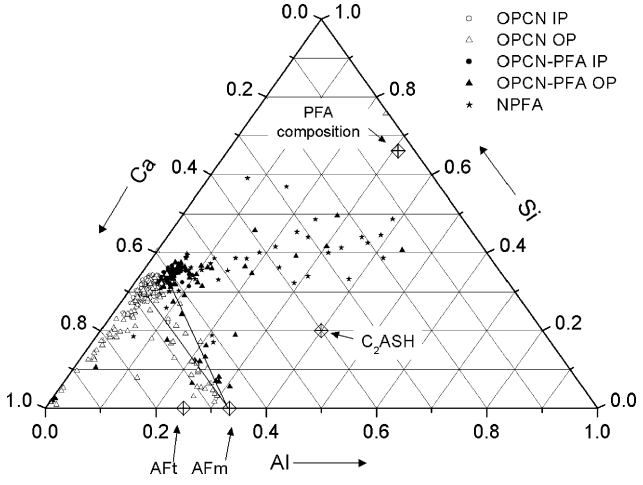


Fig. 12. Ca–Si–Al ternary diagram for OPCN and OPCN–PFA cured for 1 year at 10 and 60 °C.

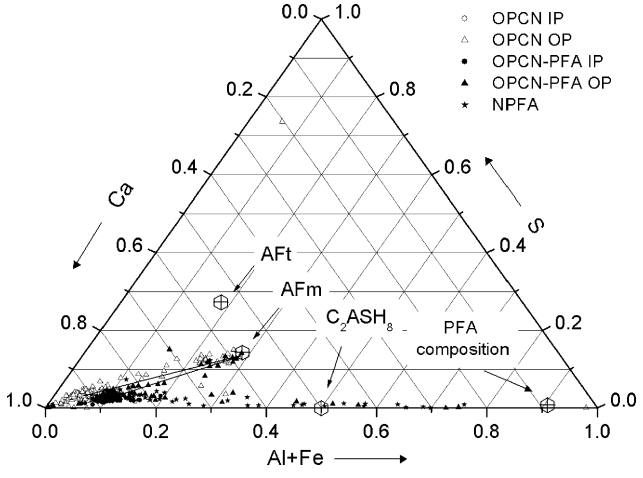


Fig. 13. Ca–S–(Al + Fe) ternary diagram for OPCN and OPCN–PFA cured for 1 year at 10 and 60 °C.

product identified by XRD in the hydrated OPC–PFA blends at both extremes of the temperature range. This trend is also apparent in Fig 13, which shows the ternary composition diagram for Ca–S–(Al + Fe). Many OP analyses fall close to the line joining the composition of C–S–H to that of AFm, but some of them and the NPFA analyses pass through the composition of stratlingite and continue towards that of the anhydrous PFA itself.

## 4. Final discussion and conclusions

The incorporation of a replacement material modified the chemical composition of the inner products of the cement fraction in all three composite cements studied during this investigation. These changes are particularly well demonstrated by representation in ternary composition diagrams, such as those already shown and are summarised in Fig. 14. In the outer products, intimate mixtures of C–S–H, AFm and CH, sometimes with additional phases (AFt, $C_2ASH_8$, hydrotalcite), were indicated.

Pozzolanic activity, associated with replacement materials, involves the uptake of $Ca^{2+}$ ions necessary for the formation of additional C–S–H gel. The resulting

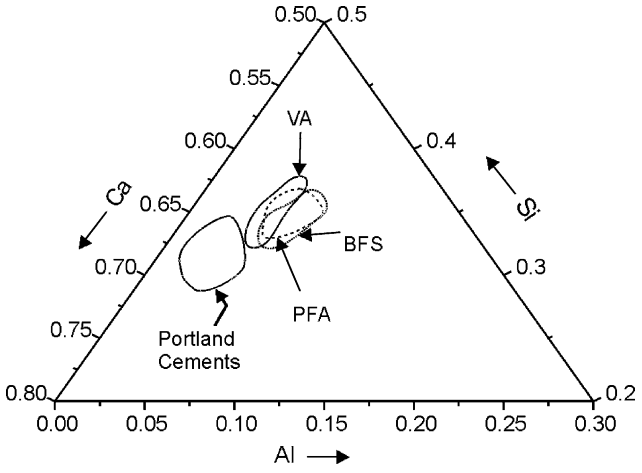


Fig. 14. Ca–Si–Al ternary diagram for inner products in neat and blended cements.

differences in the chemical composition of the inner product C–S–H in the various composite cements relative to that present in the neat cements are shown in Table 2, as averages of all studied temperatures. It can be seen that the calcium content decreased in the blended cements, while the silicon and aluminium contents increased, leading to considerable changes in the ratios of Ca/Si and Al/Ca. (N.B. the Ca/Si ratios listed have been determined using a third decimal place that is not shown in Table 2.)

Two further points can be made. One is that the magnitude of the Ca/Si ratio, if used exclusively, can disguise whether any increase is due to an increase in the numerator, a decrease in the denominator, or both. For example, the data for both the neat cements indicated that the amount of calcium was almost constant with change in curing temperature, whereas the aluminium content decreased with increasing temperature, while that of silicon and especially that of sulfur increased [8].

The second point is that the ratio of 2.12 shown in Table 2 for the Ca/Si ratio for the inner product found in the neat cements is at the upper end of those published in the literature [1]. It may be that the relatively high voltage used (20 kV) resulted in the area being analysed included some CH or even unreacted alite [1]. However, even at lower voltages it is possible to include the latter phases in the excited volumes since it is not possible to know what is underneath the two dimensional images used to select the spots for analysis. Moreover, Ca/Si ratios estimated indirectly by using quantitative X-ray diffraction analysis and thermogravimetry data [21] provided remarkably good correspondence with the ratios determined by EDS. The ratio may, therefore, be a valid determination for these cements, but the key point is that the relative differences in the Ca/Si ratios of the blended cements when compared with those for the neat cements are believed to be of the right order of magnitude, since they all were all determined under comparable experimental conditions. It was observed that the Ca/Si ratio decreased as compared with the plain Portland cement system in the presence of the replacement material (Table 2), and that the values observed were similar for each of the blended cements incorporating GGBS(60%), VA(22%) and PFA(30%).

Table 2
Average chemical composition of the C–S–H gel (IP) in the various cements (normalized to 100)

| | Ca | Si | Al | Ca/Si | Al/Ca |
|---|---|---|---|---|---|
| Neat | 0.66 | 0.31 | 0.031 | 2.12 | 0.047 |
| OPCN/BFS | 0.60 | 0.34 | 0.060 | 1.73 | 0.101 |
| OPCS–VA | 0.61 | 0.35 | 0.045 | 1.76 | 0.074 |
| OPCN–PFA | 0.60 | 0.35 | 0.054 | 1.72 | 0.091 |

## Acknowledgements

J.-I. Escalante-Garcia gratefully acknowledges financial support from the National Council of Science and Technology (CONACYT, Mexico) and the British Cement Association. The cements and chemical analyses were kindly supplied by Cementos Apasco, and the GGBS by Frodingham Cement. We wish to thank Dr R. Yang and Miss D. Bussey for their assistance in the operation of the scanning electron microscope, and Prof S. Diamond, Dr R. Yang and Dr J. Hill for helpful discussions.

## References

[1] Taylor HFW. Cement chemistry. 2nd ed. London: Thomas Telford; 1997.
[2] Kjellsen KO, Detwiler RJ, Gjorv OE. Backscattered electron imaging of cement pastes hydrated at different temperatures. Cem Concr Res 1990;20:308–11.
[3] Kjellsen KO, Detwiler RJ, Gjorv OE. Development of microstructure in plain cement pastes hydrated at different temperatures. Cem Concr Res 1991;21:179–89.
[4] Kjellsen KO, Detwiler RJ. Pore structure of plain cement pastes hydrated at different temperatures. Cem Concr Res 1992;22:112–20.
[5] Cao Y, Detwiler RJ. Backscattered electron imaging of cement pastes cured at elevated temperatures. Cem Concr Res 1995;25:627–38.
[6] Escalante-Garcia JI, Sharp JH. Effect of temperature on the hydration of the main clinker phases in Portland cements: Part I, Neat cements. Cem Concr Res 1998;28:1245–57.
[7] Escalante-Garcia JI, Sharp JH. The microstructure and mechanical properties of blended cements hydrated at various temperatures. Cem Concr Res 2001;31:695–702.
[8] Escalante-Garcia JI, Sharp JH. Variation in the composition of C–S–H gel in Portland cement pastes cured at different temperatures. J Am Ceram Soc 1999;82:3237–41.
[9] Escalante-Garcia JI, Sharp JH. The effect of temperature on the early hydration of Portland cement and blended cements. Adv Cem Res 2000;12:121–30.
[10] Escalante-Garcia JI, Sharp JH. Effect of temperature on the hydration of the main clinker phases in Portland cements: Part II, Blended cements. Cem Concr Res 1998;28:1259–74.
[11] Harrisson AM, Winter NB, Taylor HFW. An examination of some pure and composite Portland cement pastes using scanning electron microscopy with X-ray capabilities. Proc 8th Intl Congr Chem Cein, Rio de Janeiro, 1986;4:170–75.
[12] Bonen D, Diamond S. Interpretation of compositional patterns found by quantitative energy dispersive X-ray analysis for cement paste constituents. J Am Ceram Soc 1994;77(7):1875–82.
[13] Diamond S, Bonen D. Microstructure of hardened cement paste—a new interpretation. J Am Ceram Soc 1993;76(12):2993–9.
[14] Scrivener KL, Patel HH, Pratt PL, Parrot LJ. Analysis of phases in cement paste using backscattered electron images, methanol absorption and thermogravimetric analysis, in Struble LJ, Brown, PW, editors. Microstructural development during cement hydration. Mat Res Soc Symp Proc, 1986;85:67–76.
[15] Zhao H, Darwin D. Quantitative backscattered electron analysis of cement paste. Cem Concr Res 1992;22:696–706.
[16] Bustos-Martinez JL, Escalante-Garcia JI. Unpublished results.
[17] Escalante JI, Gomez LY, Johal KK, Mendoza G, Mancha H, Mendez J. Reactivity of blast furnace slag in portland cement blends hydrated under different conditions. Cem Concr Res 2001;31:1403–9.
[18] Hill J, Sharp JH. The mineralogy and microstructure of three composite cements with high replacement levels. Cem Concr Compos 2002;24:191–9.
[19] Escalante-Garcia JI, Fuentes AF, Gorokhovsky A, Fraire-Luna PE, Mendoza-Suarez G. Hydration products and reactivity of blast furnace slag activated by various alkalis. J Am Ceram Soc 2003;86(12):2148–53.
[20] Brindley GW, Kikkawa S. Am Mineral 1979;64:836–48.
[21] Escalante-Garcia JI, Mendoza G, Sharp JH. Indirect determination of the Ca/Si ratio of the C–S–H gel in Portland cements. Cem Concr Res 1999;29:1999–2003.